Theoretical Studies of Mixed-Valence Transition Metal Complexes for Molecular Computing

Sonja B. Braun-Sand and Olaf Wiest*

Department of Chemistry and Biochemistry, University of Notre Dame, Notre Dame, Indiana 46556-5670

Received: July 24, 2002; In Final Form: November 5, 2002

Possible molecular implementations of quantum-dot cellular automata (QCA) with mixed-valence ruthenium complexes are discussed. A study of the geometric and electronic structures of three mixed-valence ruthenium dimers has been done using ab initio Hartree−Fock and hybrid density functional methods at the HF/3-21G and B3LYP/3-21G levels of theory. These complexes are representatives of Robin and Day classes I, II, and III. Predicted geometries are compared to experimental data, as well as previous computational studies, where available. The B3LYP method predicts structures in better agreement with experiment than the HF method. The analysis of the orbital energies and localization provides insights into the degree of localization and the Robin−Day classification. They are therefore useful tools for the design of mixed valence compounds for use in molecular QCA.

Introduction

Since the early 1970s, the number of computing elements on a chip has doubled approximately every 18 months, following Moore's law. It has been predicted that the theoretical size limit will be reached soon, possibly by the year 2017.[1] When the limit is reached, heat dissipation and quantum effects such as electron tunneling through barriers will interfere with function. To continue following Moore's law, new computing paradigms may be needed. Several ideas have been proposed,[2−4] including quantum-dot cellular automata or QCA. QCA was first proposed as a square with clusters of metal atoms composing each corner.[5] When two extra electrons are added to the square, they occupy opposite corners because of Coulombic repulsion, as is shown in Figure 1. The two different states correspond to two energetically degenerate but distinguishable quantum states that could serve as a 1 and 0 in binary code. The electrons are then able to tunnel between the two states to perform the computation, leading to possible speed increases of 100−10 000-fold over today's processors.[6] An interesting property of this system is that it can also function as a molecular wire when a line of these cells is positioned on a surface. As shown in Figure 2, an input, or bias, on one end of the wire causes the electrons to switch so that it is in the lowest energy state. This induces a switch in the neighboring cell, and the electrostatic signal travels down the wire. If the input is changed, all of the cells in the wire will also change.

The function of QCA has been demonstrated[7] using squares that were fabricated from metal particles and were about 60 nm per side,[5] but the system must be cooled to 0.1 K to prevent random switching. For the system to operate at room temperature, the size of the squares must be reduced to 20−30 Å per side.[8] This is a demonstration of the particle-in-a-box problem. The smaller the squares are, the larger the difference between energy levels becomes. A potential problem of this approach is making metal clusters small enough to operate at room temperature. In addition, on this size scale, it becomes difficult
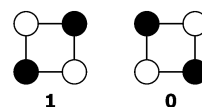
* To whom correspondence should be addressed. E-mail address: owiest@nd.edu.

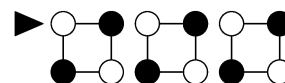**Figure 1.** Bistable cell states.

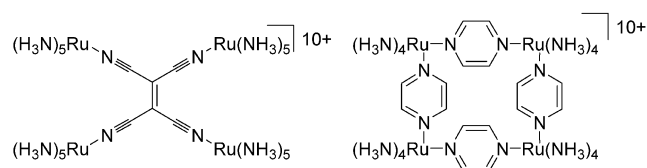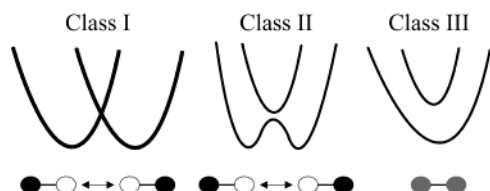**Figure 2.** Input and signal down a "wire".

Figure 3. Examples of center-bridged and side-bridged mixed-valence molecules.

to make the clusters identical to one another. This opens the door for replacing the metal clusters with molecules, which are easier to make reproducibly, and the desired size, 20−30 Å, is a typical size of molecules.

Replacing the metal clusters with metal atoms in a mixed valence state has been proposed.[9] All four metal atoms, or quantum dots, are then connected to each other in one of two ways, through the center or along the edges. Examples of each kind are shown in Figure 3. On the left, a tetracyanoethene bridge connects four rutheniumammines. Two of the ruthenium atoms have a formal charge of +2, and two have a formal charge of +3. The same is true for the complex on the right, in which the rutheniumammines are now connected along the edges of the square. This is a tetranuclear analogue of the well-known and often studied Creutz−Taube[10] complex. These mixed-valence complexes remain a topic of interest because of their interesting properties, and there have been many theoretical and experimental studies in recent years on the topic, as well as comprehensive reviews.[11,12]

Figure 4. Schematic potential energy surfaces for electron transfer in classes I, II, and III.

Robin and Day have divided mixed-valence compounds such as these into three different classes, class I, class II, and class III.[13] Class I complexes are localized and have a very large barrier to electron transfer between the different valences with a slow rate of transfer. Class III complexes are delocalized with no barrier to electron transfer and ultrafast rates. Class II complexes have properties intermediate to these. It is thought that Class II or Class III complexes may function as QCA cells. The potential energy surfaces for each class are shown schematically in Figure 4. Class II is likely the ideal case for molecular computing. The Class III complexes may be too delocalized, and unwanted electron transfer may occur at room temperature because the barrier to transfer is too low. For Class I complexes, the barrier to electron transfer is too high such that the complex is permanently "locked" in one position. Class II complexes are the most likely to be able to maintain their "1" or "0" state without undesirable electron transfer yet have a barrier low enough that it can switch when induced. The use of transition metal complexes is attractive because the electronic properties can be tuned by varying the bridging, as well as the ancillary, ligands.

One of the best known examples of mixed-valence complexes is the Creutz–Taube ion, decaammine(μ-pyrazine)diruthenium-(5+), **1**, which is widely believed to be a Robin–Day class III complex. There have been a considerable number of computational studies of **1**, which were instrumental in shaping the models for intramolecular electron transfer.[11,14–39] Work by Broo and Larson[33] used semiempirical and ab initio techniques with C_{2v} symmetry imposed on the mixed-valence complex, which forces the geometry to be delocalized. CASSCF and CNDO/S were used to calculate the electronic spectrum of the Creutz–Taube complex. More recently, work by Bencini et al.[35] uses gradient-corrected DFT, but also uses the frozen core (FC) approximation for all atoms. In addition, C_{2v} symmetry was imposed during geometry optimization and C_s symmetry during analysis of the potential energy surface, which forces the complex into a delocalized structure. In contrast, the work presented here uses an all-electron basis set (3-21G) on all atoms, including ruthenium. The paper by Chen et al.[34] uses the Amsterdam density functional package's nonlocal corrections with Becke's nonlocal exchange correction and Perdew's nonlocal correlation correction to calculate the Creutz–Taube ion similar to what is done here; however, Chen constrains the complex to C_s symmetry. Sizova et al.[29] calculated the molecular orbitals and electronic spectra of **1**, as well as the higher homologue, decaammine(μ-4,4′-bipyridine)diruthenium(5+), **2**, at frozen geometries. Other computational studies of **2** [26,28,33,40] also employed relatively low levels of theory or structural constraints or both. To the best of our knowledge, there are no computational studies of analogous compounds in which the electronic coupling between the ruthenium atoms is even weaker than that in **2**.

Because of the interest in mixed valence, homometallic complexes as molecular implementations of QCA, we have studied representatives of the three Robin–Day classes. In particular, we investigated **1** and **2** as representatives of Robin–Day classes III and II, respectively. Because of its analogous structure but weak coupling due to the absence of π bonds, we chose decaammine(μ-piperazine)diruthenium(5+), **3**, as an example for a Class I compound, even though **3** has not yet been described in the literature. The goal of this contribution is to develop a simple model of the electronic structure in a molecular QCA cell that can qualitatively correlate the structure of the complex with its intramolecular electron-transfer properties. Two different properties were examined, the ability of computational methods to predict the molecular geometries and a qualitative analysis of the molecular orbitals. The geometric and electronic ground-state structure of the complexes could in the future be used for atomistic and mesoscale simulations of QCA cells and of larger devices. For this purpose, we will start our discussion with a validation of our computational methodology for the well-known case of **1** and apply the analysis on the other homologues.

Computational Details

All calculations were performed using the Gaussian 98 series of programs.[41] The large size of these complexes made post-HF treatments such as CI, which would consider the two-configuration nature of **1**–**3**, prohibitively expensive. Gradient-corrected DFT has been used previously to describe the properties of mixed-valence complexes with both localized[42] and delocalized[43] electrons. Specifically, the Creutz–Taube complex has previously been calculated using DFT, despite the fact that it was constrained to C_s symmetry, which forces an exact degeneracy of the orbitals. However, pure DFT methods are known to be biased toward delocalized structures. This can be countered by admixture of HF exchange. The resulting hybrid DFT methods typically perform significantly better than nonlocal DFT methods.[44] Therefore, the hybrid DFT method B3LYP was chosen. B3LYP has been shown to perform well with many difficult chemical problems, including open-shell transition metal chemistry; therefore, all structures were fully optimized and characterized at the B3LYP level of theory with a 3-21G basis set on all atoms, including ruthenium. All geometries, including the HF-optimized geometry, were fully optimized without imposing symmetry, using the unrestricted Hartree–Fock (UHF) method, and were verified by harmonic frequency analysis to be true local minima with no negative frequencies. The C_2 symmetric structure for the 4,4′-bipyridine-bridged complex and the C_i symmetric piperazine-bridged complex have also been calculated. We found that imposing symmetry on the complexes in general resulted in an increase in energy of about 7 eV and a Ru–bridging ligand N bond length increase of about 0.2 Å. A symmetric pyrazine-bridged complex has also been studied by others.[33–35] Because of the ground-state nature of all processes involved in QCA computing, only the ground-state equilibrium geometry was considered. The 3-21G basis set was chosen as a reasonable compromise between the accuracy and size of the calculation (for the systems discussed here between 290 and 352 basis functions). For comparison to older work,[26,28,33,40] the 4,4′-bipyridine-bridged structure was also optimized at the HF level of theory with a 3-21G basis set on all atoms. All bond lengths are given in angstroms. The nitrogen atoms will be distinguished from one another by the following convention: N_{BL} will be used for the N atoms on the bridging ligand, N_a for the axial N atoms, and N_e for the equatorial N atoms. In addition, HF/3-21G single-point calculations were done on the B3LYP/3-21G optimized geometries to obtain the molecular orbitals, for reasons that will be discussed later in
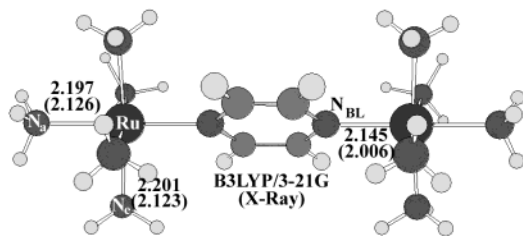
Figure 5. Selected theoretical and X-ray[48] (in parentheses) bond lengths of the class III complex **1**.
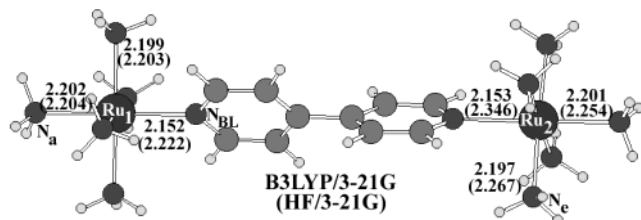
Figure 6. B3LYP/3-21G and HF/3-21G (in parentheses) bond lengths for the class II complex **2**.
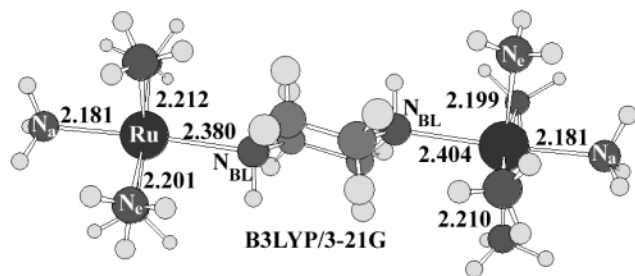
Figure 7. B3LYP/3-21G bond lengths for the class I complex **3**.

the paper. The polarization of the complexes was gauged using Mulliken charges. Basis-set-derived population analyses (such as Mulliken charge) are most useful for trend comparison, as used here, rather than an estimate of the actual value.[45] The molecular orbital representations were viewed and created with MOLDEN, using a contour value of 0.05.[46]

Results and Discussion

Structural Analysis. The theoretically obtained geometries are shown in Figures 5−7 and compared with the available experimental data. Figure 5 shows **1**, which is most often regarded as Class III[47] though recently it has been suggested that a separate characterization is needed for species such as these, called Class II−III.[47] An X-ray crystal structure of this complex is available for comparison,[48] and the experimentally determined bond lengths are shown in Figure 5. These results are very similar to the results obtained by Chen et al.,[34] as can be seen in Table 1. In general, the computed bond lengths are overestimated, especially between the ruthenium atoms and the bridging ligand. This is not surprising because the metal centers have high positive charges and Coulomb repulsion is enhanced in these gas-phase calculations. There is a slightly better agreement between theory and experiment for the bond lengths between the ruthenium atoms and terminal amines. The Ru−N_a bond lengths are equal on both sides, suggesting that the ruthenium atoms have the same valence. The Ru−N_e bond lengths vary from 2.200 to 2.202 Å with the average bond length 2.201 Å. The Ru−N_{BL} bond lengths are equal on both sides of the complex, 2.145 Å, also suggesting complex delocalization.

Table 1 shows a summary of the computed geometries of this paper, as well as some computed geometries from the literature.

For comparison, the X-ray structure and computed geometries for the monomer Ru(NH$_3$)$_5$(pyrazine)$^{3+/2+}$ are given in Table 2. The +2 ion typically has shorter Ru−N bond lengths.

For **2**, the structure was fully optimized using both B3LYP and HF methodology. The HF results are shown here for comparison to previous work. The 4,4′-bipyridine bridging ligand is thought to be a Class II because of its solvent-dependent near-IR spectrum and other experimental observations.[11] From the results shown in Figure 6, it is apparent that the HF method overestimates the Ru−N_{BL} bond lengths more than B3LYP (from 0.07 to 0.19 Å more). The HF calculations predict large differences in the Ru−N_{BL} bond lengths depending on the oxidation state of the metal atom, the Ru(II)−N_{BL} bond length being significantly shorter than that for Ru(III). Consistently, the bonds from the Ru(III) to N_a and N_e are also significantly longer (0.05−0.07 Å) than those for Ru(II). The Ru−N_e bond lengths calculated with B3LYP are essentially identical and vary from 2.197 to 2.200 Å, the average being 2.198 Å. With HF, the Ru(II)−N_e bond lengths are 2.203 Å and the Ru(III)−N_e bond lengths vary from 2.267 to 2.268 Å, averaging 2.267 Å. The B3LYP methodology also predicts a slight difference in the Ru−N_{BL} bond lengths though not as dramatic as that for HF. This indicates that **2** is more localized than the pyrazine-bridged species, as would be expected from a decreased conjugation between the pyridyl rings due to the tilting of the bridging bipyridine ligand, as well as the larger Ru−Ru separation. The dihedral angle between the pyridyl rings is 39° for B3LYP and 54° for HF. A crystal structure of a similar 4,4′-bipyridine-bridged ruthenium complex showed a dihedral angle of approximately 18°.[50] The HF structure again emphasizes a more localized structure in which the steric repulsion between the ortho hydrogens in the bridging ligand leads to a sharper tilting and even further localization of spin and charge. These data support the idea that this is indeed a Class II complex or at least is more localized than the pyrazine-bridged species.

The final complex **3**, Figure 7, has piperazine as the bridging ligand. This complex is not known experimentally, but because of the lack of π conjugation in the bridging ligand, it is assumed to be a Class I species. In addition, piperazine was chosen for its size similarity to pyrazine. The B3LYP-predicted Ru−N_a/N_e bond lengths are similar to those predicted for the class II and III species. The Ru−N_e bond lengths vary from 2.199 to 2.212 Å, the average being 2.205 Å. However, the Ru−N_{BL} ligand bonds are significantly longer, likely because of a lack of dπ to π* back-bonding from the metal to the ring. Even for this complex, B3LYP predicts Ru−N_{BL} bond lengths that are nearly identical, suggesting delocalization. However, B3LYP is known to overestimate delocalization, and HF is known to overestimate localization.[51−53]

Orbital Analysis. Assuming the electron transfer from one metal to the other metal occurs via the ligand, the energy gap between the singly occupied molecular orbital (SOMO) and the molecular orbital centered on the bridging ligand should give an indication of the barrier to electron transfer. There have been several recent studies about superexchange in mixed-valence ruthenium dimers.[54−56] These studies have suggested that there is stronger metal−metal coupling when the energy gap between the molecular orbital on the ligand and the dπ-orbitals on the metal atoms is small. Figure 8 shows the SOMO, as well as the bridging ligand molecular orbital (BLMO) of **1**. The BLMO corresponds to the lowest unoccupied molecular orbital (LUMO) with an energy gap of 8.16 eV. The SOMO is located on both

**TABLE 1: Summary of Computed and Experimental Bond Lengths**

	B3LYP/3-21G[a]	X-ray[48]47	BP[35,b]		BP[35,b]		BP[34]	INDO/1[33]
			nonrelativistic	relativistic	nonrelativistic	relativistic		
Ru−Ru	7.185	6.841	7.294	7.185	6.923	6.892	nr	nr
Ru(1)−N$_{BL}$	2.145	2.006	2.203	2.134	2.026	1.998	2.148	2.056
Ru(2)−N$_{BL}$	2.145	2.006	2.203	2.134	2.026	1.998	2.148	2.067
Ru−N$_a$	2.197	2.126	2.162	2.154	2.116	2.108	2.200/2.205	2.079/2.094
Ru−N$_e$	2.201	2.122	2.176	2.159	2.120	2.109	2.197	2.085/2.096

^{a} Results from this paper. ^{b} BP is the Becke−Perdew method, as modified in ref 35. Reference 35 also compared results of calculations that did or did not include relativistic effects.

TABLE 2: Summary of Computed and Experimental Bond Lengths for Ru(NH$_3$)$_5$(pyrazine)$^{+3/+2}$

	B3LYP/3-21G[a]		HF/3-21G[a]		BP[34]		INDO/1 [33]	X-ray [49]	
	+3	+2	+3	+2	+3	+2	+2	+3	+2
Ru−N$_{BL}$	2.155	2.085	2.434	2.238	2.136	2.078	2.041	2.076	2.006
Ru−N$_a$	2.206	2.223	2.238	2.265	2.213	2.247	2.099	2.125	2.116
Ru−N$_e$	2.192−2.195	2.202/2.203	2.271−2.274	2.266/2.267	2.193	2.195/2.199	2.092	2.102/2.110	2.150/2.155

^{a} Results from this paper.
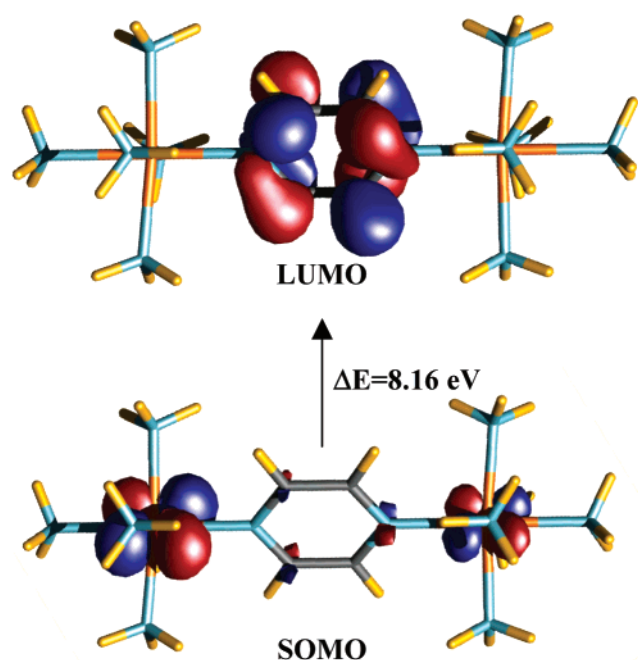
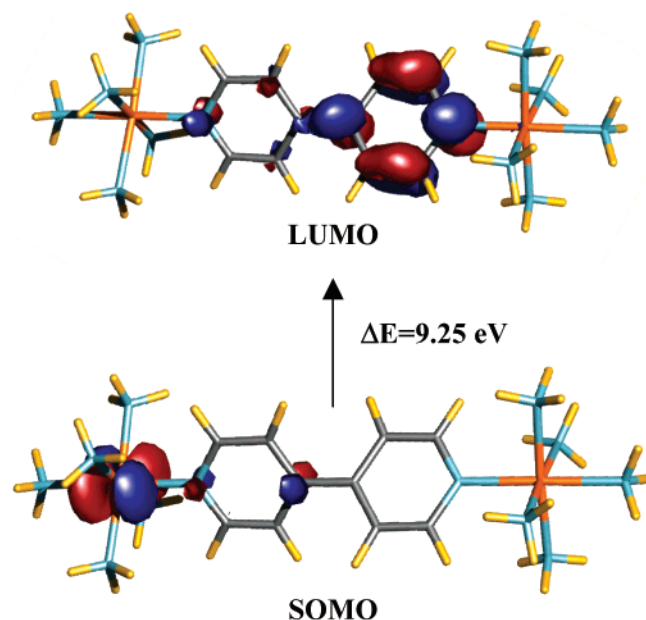**Figure 8.** HF orbitals of **1**.

Figure 9. KS orbitals of **1**.

ruthenium atoms, as would be expected for a delocalized complex. The Mulliken spin density on each Ru is −0.03 and 0.05; the Mulliken charge on each Ru is 0.85 and 0.86. Considering the fact that HF tends to overestimate localization, this is a good indication of the delocalized nature of this complex. These calculations support that **1** is a Robin−Day class III complex.

As previously mentioned, a HF/3-21G single-point calculation was done on the B3LYP/3-21G fully optimized geometries for the orbital analysis. Although the Kohn−Sham (KS) orbitals obtained from B3LYP calculations reproduce the ground-state electron density of the complex, their physical significance is not well understood and has recently become a topic of much study.[57] For this reason, our discussion will focus on the HF orbitals. For comparison, the KS orbitals are given in Figure 9. Much as Hoffmann and Stowasser found, the shape of the KS orbitals are very similar to those calculated with the HF method. With the small basis set used here, there was some evidence of orbital interchange among the empty orbitals, as can be seen for the case of **3** in Figures 12 and 13. Hoffmann and Stowasser
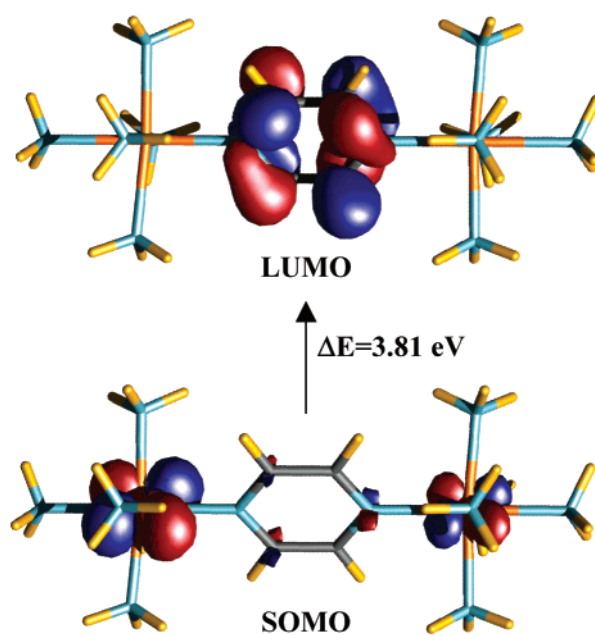
also suggested that occupied and unoccupied KS orbitals can be interpreted quantitatively with an $ax + b$ scaling, but this was not investigated here.

Figure 10 shows the molecular orbitals for **2**. The SOMO−LUMO gap is slightly larger here, 9.25 eV. The SOMO on this complex is located on just one of the ruthenium atoms, suggesting more localization than the Class III complex. The molecular orbital centered on the bridging ligand is also the LUMO. In contrast to the Class III complex, this orbital is no longer spread out equally on all of the bridging ligand atoms because of the break in the π conjugation between the pyridyl rings. The orbital localization due to the weaker interaction with the bridging orbital is also reflected in the difference in Mulliken spin density on each Ru, which is larger here, 0.00 and 1.14. The difference in Mulliken charge is also larger, 0.86 and 1.18. These results indicate that this is not a class III complex but probably class II. The Kohn−Sham (KS) orbitals are shown in Figure 11. It is noteworthy that, in comparison with the KS orbitals of **1** and **3**, the relative bias of the HF and DFT methodology has a larger influence on the LUMO of this class II complex. Whereas the shape of the HF and KS orbitals

Figure 10. HF orbitals of **2**.
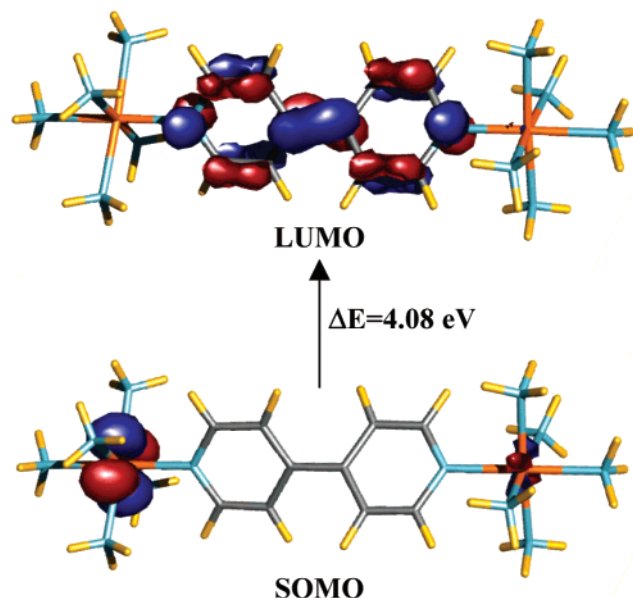
Figure 11. KS orbitals of **2**.

calculated for **1** are very similar, KS theory predicts a much larger degree of delocalization for the LUMO of **2**. This is consistent with the expectation that the bias of the different theoretical methods should be most clearly observed for a partially delocalized class II complex. Nevertheless, it is clear from the very similar SOMO orbitals obtained by the two methods that these differences are quantitative rather than qualitative in nature.

Complex **3**, shown in Figure 12, is substantially different than the other two complexes. The SOMO of this complex is actually on the bridging ligand. The highest occupied metal-centered orbital, which constituted the SOMO in **1** and **2**, is slightly lower in energy, making it the SOMO-1. Of the three complexes, this has the largest gap between the highest occupied metal-centered orbital (SOMO-1) and the BLMO, 19.3 eV. The SOMO–BLMO gap is also large, 18.4 eV. The BLMO is no longer the LUMO and is located much higher in the orbital ordering, LUMO + 12. This is because piperazine has only σ and no π bonds. The σ^* orbitals lie much higher in energy than π^*

orbitals, leading to these very large energy gaps. The lowest-lying molecular orbital on the opposite ruthenium atom is now the LUMO + 5, and the energy gap between this and the SOMO-1 is 16.1 eV. The electronic coupling between the two metal centers is thus predicted to be weak, as expected for a Class I compound. The difference in Mulliken spin density on each Ru is very small, 0.54 on each, because of the SOMO being located on the bridging ligand. The difference in Mulliken charge is also small, approximately 0.93 on each ruthenium. The Kohn–Sham orbitals are shown in Figure 13 for comparison. It can be noted that, although significant energetic orbital reordering occurs, the shapes of the relevant orbitals are quite similar. In fact, in the KS orbitals, the SOMO is centered on a single ruthenium atom as would be expected on the basis of the results for **1** and **2**. The lowest-lying unoccupied bridging ligand orbital is the LUMO + 12, as it is in the HF calculation. These results indicate that orbital calculations can distinguish between the three Robin and Day classes, provided that the electron transfer proceeds through the bridging ligand. The class III, strong coupling complexes appear to have significant contributions from both metal atoms in the SOMO, while the class II and I complexes have the SOMO centered on only one metal atom. For class I, the LUMO is no longer on the bridging ligand.

Conclusions

The results of the bonding studies show that both methods, B3LYP and HF, overestimate bond lengths compared to X-ray crystal structure data because of Coulomb repulsion in the gas phase. HF emphasizes the differences between Ru(II) and Ru(III), which gives a more localized picture of the complexes than B3LYP. However, the results from the B3LYP calculations for the critical C–N$_B$ bond length are in better agreement with experimental values than those from the HF calculations.

The results of the MO calculations help to distinguish among the three Robin and Day classes. Class III complexes have significant contributions from both metal atoms in the SOMO, while class II complexes have the SOMO centered on only one metal atom. For class I complexes, both ruthenium atoms seem to prefer a formal charge of +2 with the unpaired electron located on the bridging ligand. For class I, the LUMO is no longer on the bridging ligand. The energy gap between the SOMO and BLMO increases consistently as the complex becomes more localized, and the BLMO is also the LUMO for more delocalized complexes but higher for more localized complexes. The result can be used to qualitatively evaluate the electronic communication between the metal centers in the mixed-valence complexes, and therefore, their suitability as molecular implementations of QCA can be determined before compounds are synthesized. This will be useful in designing new QCA molecules with improved properties.

In future studies, the change in electronic properties as the bridging or ancillary ligands of the complexes are substituted will be examined by us, as well as intercell communication[58] and eventually device simulation. Future work on these interesting complexes includes alternate computational treatments such as MP2 or GVB-PP, using an active space of the SOMO and LUMO orbitals, to obtain further insights into the effect of electron correlation on electron localization vs delocalization.
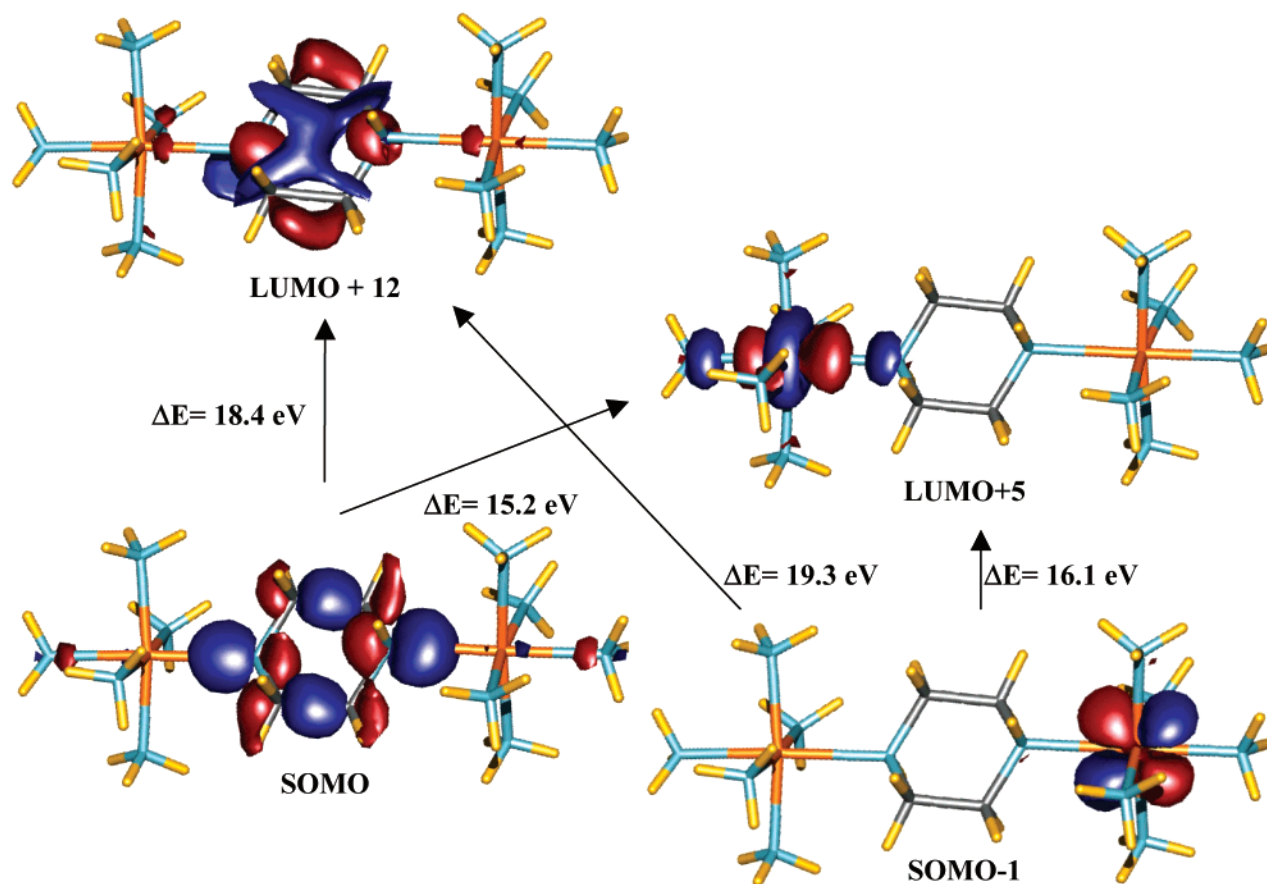
Figure 12. HF orbitals of **3**.
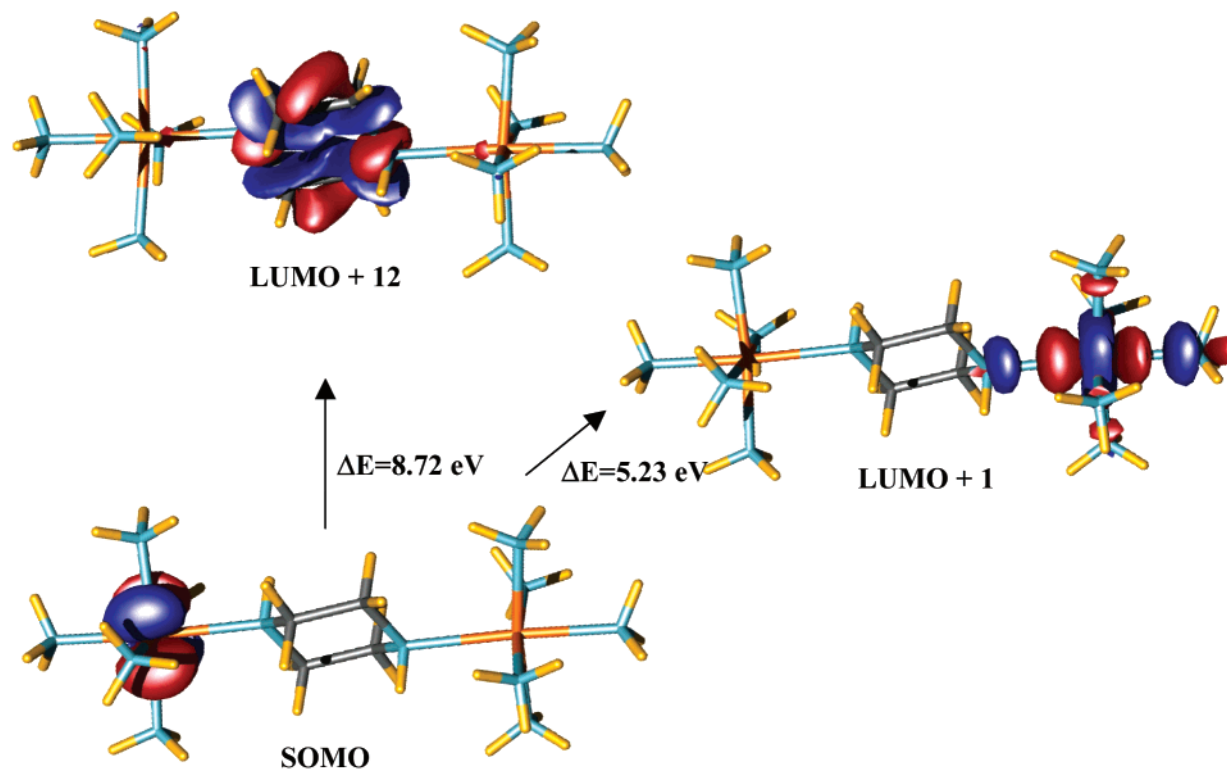
Figure 13. KS orbitals of **3**.

Supporting Information Available: The Cartesian coordinates of all fully optimized complexes. This material is available free of charge via the Internet at http://pubs.acs.org.

Mixed-Valence Transition Metal Complexes

J. Phys. Chem. A, Vol. 107, No. 2, 2003 **291**

References and Notes

(1) Reed, M. A.; Tour, J. M. *Sci. Am.* **2000**, *282*, 86−93.

(2) Reed, M. A.; Zhou, C.; Muller, C. J.; Burgin, T. P.; Tour, J. M. *Science* **1997**, *278*, 252−254.

(3) Collier, C. P.; Wong, E. W.; Belohradsky, M.; Raymo, F. M.; Stoddart, J. F.; Kuekes, P. J.; Williams, R. S.; Heath, J. R. *Science* **1999**, *285*, 391−394.

(4) Ellenbogen, J. C.; Love, J. C. *P. IEEE* **2000**, *88*, 386−426.

(5) Orlov, A. O.; Amlani, I.; Bernstein, G. H.; Lent, C. S.; Snider, G. L. *Science* **1997**, *277*, 928−930.

(6) Glanz, J. *Science* **1995**, *269*, 1363−1364.

(7) Amlani, I.; Orlov, A. O.; Toth, G.; Bernstein, G. H.; Lent, C. S.; Snider, G. L. *Science* **1999**, *284*, 289−291.

(8) Snider, G. L.; Samuelson, L. Unpublished results.

(9) Lieberman, M.; Chellamma, S.; Varughese, B.; Wang, Y.; Lent, C.; Bernstein, G. H.; Snider, G.; Peiris, F. C. *Ann. N. Y. Acad. Sci.* **2002**, *960*, 225−239.

(10) Creutz, C.; Taube, H. *J. Am. Chem. Soc.* **1973**, *95*, 1086−1094.

(11) Creutz, C. *Prog. Inorg. Chem.* **1983**, *30*, 1−73.

(12) Crutchley, R. J. *Adv. Inorg. Chem.* **1994**, *41*, 273−325.

(13) Robin, M. B.; Day, P. *Adv. Inorg. Chem. Radiochem.* **1967**, *10*, 247−422.

(14) Wong, K. Y.; Schatz, P. N. *Prog. Inorg. Chem.* **1981**, *28*, 369−449.

(15) Piepho, S. B.; Krausz, E. R.; Schatz, P. N. *J. Am. Chem. Soc.* **1978**, *100*, 2996−3005.

(16) Root, L. J.; Ondrechen, M. J. *Chem. Phys. Lett.* **1982**, *88*, 538−542.

(17) Ferretti, A.; Lami, A.; Ondrechen, M. J.; Villani, G. *J. Phys. Chem.* **1995**, *99*, 10484−10491.

(18) Murga, L. F.; Ferretti, A.; Lami, A.; Ondrechen, M. J.; Villani, G. *Inorg. Chem. Commun.* **1998**, *1*, 137−140.

(19) Ko, J.; Ondrechen, M. J. *J. Am. Chem. Soc.* **1985**, *107*, 6161−6167.

(20) Root, L. J.; Ondrechen, M. J. *Chem. Phys. Lett.* **1982**, *93*, 421−424.

(21) Linderberg, J.; Ratner, M. A. *J. Am. Chem. Soc.* **1981**, *103*, 3265−3271.

(22) Schatz, P. N.; Piepho, S. B.; Krausz, E. R. *Chem. Phys. Lett.* **1978**, *55*, 539−542.

(23) Piepho, S. B. *J. Am. Chem. Soc.* **1988**, *110*, 6319−6326.

(24) Piepho, S. B. *J. Am. Chem. Soc.* **1990**, *112*, 4197−4206.

(25) Borshch, S. A.; Kotov, I. N. *NATO ASI Ser., Ser. C* **1991**, *343*, 347−352.

(26) Ferretti, A.; Lami, A.; Villani, G. *Inorg. Chem.* **1998**, *37*, 2799−2805.

(27) Kuznetsov, A. M.; Ulstrup, J. *J. Chem. Phys.* **1981**, *75*, 2047−2055.

(28) Lauher, J. W. *Inorg. Chim. Acta* **1980**, *39*, 119−123.

(29) Sizova, O. V.; Baranovskii, V. I.; Panin, A. I.; Ivanova, N. V. *J. Struct. Chem.* **1999**, *39*, 471−479.

(30) Leshchev, D. V.; Baranovskii, V. I.; Sizova, O. V.; Panin, A. I. *J. Struct. Chem.* **2000**, *40*, 493−502.

(31) Ondrechen, M. J.; Ellis, D. E.; Ratner, M. A. *Chem. Phys. Lett.* **1984**, *109*, 50−55.

(32) Zhang, L. T.; Ko, J.; Ondrechen, M. J. *J. Am. Chem. Soc.* **1987**, *109*, 1666−1671.

(33) Broo, A.; Larsson, S. *Chem. Phys.* **1992**, *161*, 363−378.

(34) Chen, Z.; Bian, J.; Zhang, L.; Li, S. *J. Chem. Phys.* **1999**, *111*, 10926−10933.

(35) Bencini, A.; Ciofini, I.; Daul, C. A.; Ferretti, A. *J. Am. Chem. Soc.* **1999**, *121*, 11418−11424.

(36) Murga, L. F.; Ondrechen, M. J. *Theor. Chim. Acta* **1995**, *90*, 331−339.

(37) Hush, N. S. *Chem. Phys.* **1975**, *10*, 361−366.

(38) Zhang, L. T.; Ko, J.; Ondrechen, M. J. *J. Phys. Chem.* **1989**, *93*, 3030−3034.

(39) Ondrechen, M. J.; Ko, J.; Root, L. J. *J. Phys. Chem.* **1984**, *88*, 5919−5923.

(40) Woitellier, S.; Launay, J. P.; Joachim, C. *Chem. Phys.* **1989**, *131*, 481−488.

(41) Frisch, M. J.; Trucks, G. W.; Schlegel, H. B.; Scuseria, G. E.; Robb, M. A.; Cheeseman, J. R.; Zakrzewski, V. G.; Montgomery, J. A., Jr.; Stratmann, R. E.; Burant, J. C.; Dapprich, S.; Millam, J. M.; Daniels, A. D.; Kudin, K. N.; Strain, M. C.; Farkas, O.; Tomasi, J.; Barone, V.; Cossi, M.; Cammi, R.; Mennucci, B.; Pomelli, C.; Adamo, C.; Clifford, S.; Ochterski, J.; Petersson, G. A.; Ayala, P. Y.; Cui, Q.; Morokuma, K.; Malick, D. K.; Rabuck, A. D.; Raghavachari, K.; Foresman, J. B.; Cioslowski, J.; Ortiz, J. V.; Stefanov, B. B.; Liu, G.; Liashenko, A.; Piskorz, P.; Komaromi, I.; Gomperts, R.; Martin, R. L.; Fox, D. J.; Keith, T.; Al-Laham, M. A.; Peng, C. Y.; Nanayakkara, A.; Gonzalez, C.; Challacombe, M.; Gill, P. M. W.; Johnson, B. G.; Chen, W.; Wong, M. W.; Andres, J. L.; Head-Gordon, M.; Replogle, E. S.; Pople, J. A. *Gaussian 98*, Revision A9; Gaussian, Inc.: Pittsburgh, PA, 1998.

(42) Bencini, A.; Gatteschi, D.; Mattesini, M.; Totti, F.; Ciofini, I. *Mol. Cryst. Liq. Cryst. A* **1999**, *335*, 1377−1386.

(43) Barone, V.; Bencini, A.; Ciofini, I.; Daul, C. A.; Totti, F. *J. Am. Chem. Soc.* **1998**, *120*, 8357−8365.

(44) Wolfram Koch, M. C. H. *A Chemist's Guide to Density Functional Theory*; Wiley-VCH: Weinheim, Germany, 2000.

(45) Jensen, F. *Introduction to Computational Chemistry*; John Wiley & Sons: Chichester, U.K., 1998.

(46) Schaftenaar, N. G. *MOLDEN*, version 3.2. For details of this program, please see the URL http://www.caos.kun.nl/~schaft/molden.

(47) Demadis, K. D.; Hartshorn, C. M.; Meyer, T. J. *Chem. Rev.* **2001**, *101*, 2655−2685.

(48) Beattie, J. K.; Hush, N. S.; Taylor, P. R.; Raston, C. L.; White, A. H. *J. Chem. Soc., Dalton Trans.* **1977**, 1121−1124.

(49) Gress, M. E.; Creutz, C.; Quicksall, C. O. *Inorg. Chem.* **1981**, *20*, 1522−1528.

(50) Szalda, D. J.; Fagalde, F.; Kataz, N. E. *Acta Crystallogr.* **1996**, *C52*, 3013−3016.

(51) Bally, T.; Borden, W. T. *Rev. Comput. Chem.* **1999**, *13*, 1−97.

(52) Braieda, B.; Hiberty, P. C.; Savin, A. *J. Phys. Chem. A* **1998**, *102*, 7872−7877.

(53) Sodupe, M.; Bertran, J.; Rodriguez-Santiago, L.; Baerends, E. J. *J. Phys. Chem. A* **1999**, *103*, 166−170.

(54) Evans, C. E. B.; Yap, G. P. A.; Crutchley, R. J. *Inorg. Chem.* **1998**, *37*, 6161−6167.

(55) Evans, C. E. B.; Naklicki, M. L.; Rezvani, A. R.; White, C. A.; Kondratiev, V. V.; Crutchley, R. J. *J. Am. Chem. Soc.* **1998**, *120*, 13096−13103.

(56) Naklicki, M. L.; Evans, C. E. B.; Crutchley, R. J. *J. Mol. Struct.* **1997**, *405*, 87−92.

(57) Stowasser, R.; Hoffmann, R. *J. Am. Chem. Soc.* **1999**, *121*, 3414−3420.

(58) Braun-Sand, S. B.; Wiest, O., manuscript in preparation.